Applied Catalysis B: Environmental 213 (2017) 9–17

Contents lists available at ScienceDirect

Applied Catalysis B: Environmental

journal homepage: www.elsevier.com/locate/apcatb

Feature Article

A C_3N_4 surface passivated highly photoactive Au-TiO_2 tubular nanostructure for the efficient H_2 production from water under sunlight irradiation

Rayees Ahmad Rather, Satnam Singh, Bonamali Pal*

School of Chemistry and Biochemistry, Thapar University Patiala, Punjab, 147004, India

ARTICLE INFO

Article history:
Received 6 March 2017
Received in revised form 24 April 2017
Accepted 2 May 2017
Available online 2 May 2017

Keywords:
One pot hydrothermal synthesis
C_3N_4 passivated Au-TiO_2 tubular nanostructure
Self exfoliation of C_3N_4
H_2 production under direct sunlight
Photochemical and thermal stability

ABSTRACT

In context to the recent advances in the development of sunlight active nanocomposites for the renewable H_2 production from water, a C_3N_4 passivated Au-TiO_2 tubular nanocomposite (CTA) has been prepared by a facile one pot hydrothermal method. Structural and morphological studies revealed the elongated anatase TiO_2 nanotubes (200–250 nm long, d = 12 nm) embedded in a thin layer of graphitic C_3N_4 (1–3 nm) and dispersed Au (7–12 nm) nanoparticles. The bulk C_3N_4 turned into monolayer due to the self exfoliation process confirmed by Raman (G band = 1545 cm^{-1}). The potential voltage (I–V) characteristics revealed the non ohmic properties of the heterojunction with a good current response (1.385×10^{-4} A). The nanocomposite showed efficient photocatalytic activity with the production of ~88 $\mu molh^{-1}$ (*calculated* = 2933 $\mu molh^{-1}g^{-1}$) of H_2 gas under direct sunlight irradiation using methanol as hole scavenger. The C_3N_4 is activated under sunlight and simultaneously sensitized by Au due to its plasmonic effect. The band potential of C_3N_4 (-1.21 eV *vs* NHE for E_{CB}) is more negative than TiO_2 (E_{CB} = −0.29 Vs NHE) enabling photo induced electrons to easily pass the interface into the E_{CB} of TiO_2 which promotes the charge carrier separation and enhance the photocatalytic activity for H_2 production.

1. Introduction

Solar driven hydrogen production from water splitting is considered as the zero carbon emission process to tackle the exponentially increasing energy demand [1]. But the major challenge remains in finding a suitable photoactive, photostable and thermodynamically viable material to harvest the solar energy efficiently. Water splitting is an uphill reaction needing 237 kJ/mol of energy thermodynamically and also involves a difficult four electron reduction process [2]. To satisfy this condition the semiconductor photocatalyst should possess suitable conduction band potential/position, high charge separation efficiency (electrons and holes) and enough time for these to take part in the interface water reduction reaction [3,4].

In this regard titanium dioxide (TiO_2) is considered as an ideal candidate [5–7] due to its feasible reduction potential along normal hydrogen electrode (NHE), photostability and cost effectiveness but still deficiencies prevail in terms of its absorption in the UV region due to its large band gap (E_g = 3.2 eV) and low charge separation efficiency [8]. The variations like maximizing the specific surface area [9] and modification of nanosize geometries, in particular the nanorods [10] and nanotubes [11] have been reported to be in a higher control of chemical and physical behavior. The electronic properties changes drastically by changing the morphology due to the strong influence of surface curvature helping the TiO_2 to act in a more effective way. Secondly the formation of composite system with other semiconductors like C_3N_4 had been reported [12,13] to enhance the photocatalytic hydrogen evolution that is also associated with the effective charge transfer. The C_3N_4 is well known to build an electric field at the heterojunction with TiO_2 that helps to divert the electrons and holes in contrary directions owing to reduce their unfavorable recombination [14]. By building a heterojunction of different optical response (C_3N_4 and TiO_2) is also supposed to make the nanocomposite active in both UV and visible light. Incorporation of noble metal like gold (Au) nanoparticles can also act as an electron trap aiding the charge separation and also sensitizing the TiO_2 in visible light due to the localized surface plasmon resonance (LSPR) effect [15,16]. Li et al. have previously reported [17] that addition of Au nanoparticles between two semiconductors (CdS-TiO_2) is able to reduce the trap state Auger rate and partially compensates the negative effects of the surface trap sites resulting in the improved photoconversion effi-

* Corresponding author.
E-mail address: bpal@thapar.edu (B. Pal).

http://dx.doi.org/10.1016/j.apcatb.2017.05.002
0926-3373/

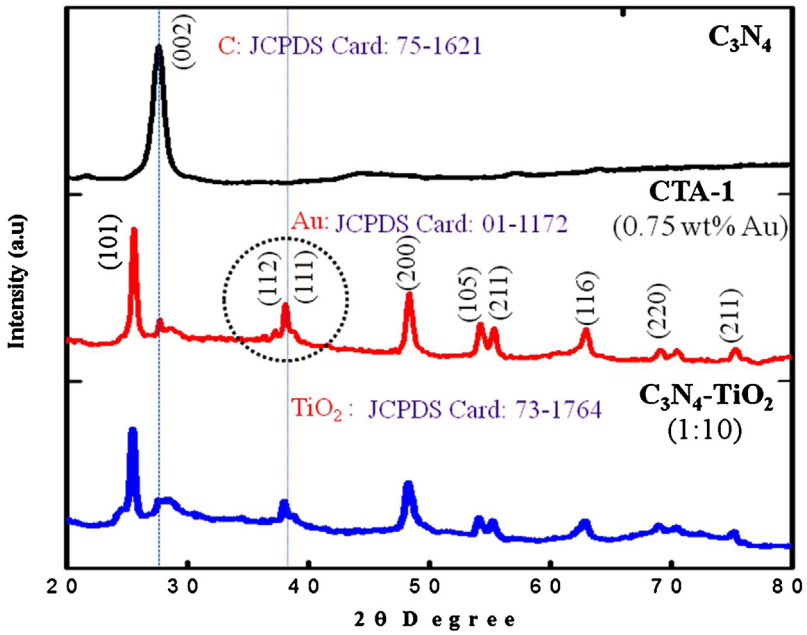

Fig. 1. X ray diffraction pattern of different photocatalysts.

ciency. The Au nanoparticles are also supposed to provide efficiency for the transport of electrons between two semiconductors. Several reports have already suggested the effective photocatalytic activity of the C_3N_4-TiO_2 [18–20] nanocomposite but the role of morphology alteration of TiO_2 into elongated nanotubes and it composite formation with C_3N_4 and simultaneous Au loading is least studied, the synthetic protocols for the same are too tedious and less efficient.

In this study a facile one step hydrothermal route was designed for the synthesis of CTA nanocomposite possessing brilliant optoelectronic and structural properties. The nanocatalyst was designed to minimize the drawbacks of TiO_2. The C_3N_4 was chosen to sensitize the TiO_2 (NT) and Au will acts both as a sensitizer and transporter of electrons. This ternary NC has shown brilliant performance for the photoreduction of water in presence of methanol as hole scavenger.

2. Experimental section

2.1. Chemicals and reagents

All the analytic grade chemicals were used as received, urea (99.5%, Loba Chemie Ltd), sodium hydroxide (NaOH, 97%, SD Fine Ltd), cetryl trimethyl ammonium bromide (CTAB, 98%, Spectrochem Pvt. Ltd), ascorbic acid (99%, Loba Chemie Ltd), chloroauric acid ($HAuCl_4$, 49% Sigma Aldrich), Ethanol (99.9%, Jingsu Huaxi International China), titanium dioxide (TiO_2-P25, 50% Evonik Industries). Deionized (DI) water from Millipore (Milli-Q an ultra filtration system with 40 mho cm^{-1} at 25 °C conductivity) was used throughout the experiment.

2.2. Preparation of carbon nitride (C_3N_4) and C_3N_4 passivated Au-TiO_2 (CTA) nanocomposite

The C_3N_4 was prepared under ambient conditions of temperature and pressure by the pyrolysis of the urea. In a typical procedure, urea (5 g) was put in a covered crucible and heated in an oven at 550 °C for 3 h to obtain a yellow colored C_3N_4.

The tubular C_3N_4 passivated Au-TiO_2 nanostructure has been synthesized by a single facile hydrothermal method (Scheme ESI-1, electronic supporting information). A 0.9 g of CTAB was dissolved in NaOH (35 mL, 10 M) and stirred till a clear solution was obtained. In another beaker TiO_2-P25 (2.5 g) and C_3N_4 (variable ratio with TiO_2-P25) was mixed with a glass rod, the mixture was added to the CTAB solution and stirred further for 10 min. The required amount of $HAuCl_4$ solution (0.01 M, corresponding to different weight percent ratios) and 0.6 g of ascorbic acid (1 M) was added and stirred vigorously for next 20 min. The mixture was hydrothermally treated in an autoclave (80 mL) at 130 °C for 24 h, the final composite was cooled at room temperature and separated under several washings of HNO_3 (0.1 M) until pH = 7 was achieved. The composite was washed with ethanol and dried at 70 °C for further analysis.

The formation of the TiO_2 nanotubes is ascribed to the one dimensional growth and exfoliation process of the TiO_2 (P25) precursor, previously it had been reported that the growth occurs through the formation of sodium titanate nanotubes [21]. Moreover, in the same strong basic medium ascorbic acid gets easily hydrolyzed to ascorbate to reduce Au^{+4} to Au^0 and CTAB helped in the stabilization of as formed Au^0 nanoparticles. The exfoliation of TiO_2 and C_3N_4 took place simultaneously to form a tubular CTA nanostructure. Later the Na^+ is removed by washing the nanocomposite several times with the HNO_3. The ratio of Au and C_3N_4 was changed to study the overall activity for the photoreduction of water, the different photocatalysts were abbreviated as CTA-1 (Au 0.75 wt%, C_3N_4:TiO_2 1:10), CTA-2 (Au 0.50 wt%, C_3N_4:TiO_2 1:10), CTA-3 (Au 0.25 wt%, C_3N_4:TiO_2 1:10), CTA-4 (Au 0.75 wt%, C_3N_4:TiO_2 3:10) and CTA-5 (Au 0.75 wt%, C_3N_4:TiO_2 5:10).

2.3. Characterization and photocatalytic activity

X-ray diffraction pattern of the photocatalyts was done with the PANalytical Xpert Pro (Almelo, Netherlands) with Cu Kα at 1.54 A° operating at 45 kV and diffraction angle of 20–80° (5°/min rise), high resolution transmission electron microscopy (HRTEM) was carried out on Technie G2 (FEI) S-Twin instrument operated at 200 kV transmission. The optical properties were studied by Analytic Jena, Specord 205 (Germany) UV–vis spectrometer and the photoluminescence (PL) on Perkin Elmer LS 55 with excitation wavelength at 320 nm. X ray photon spectroscopy (XPS) was

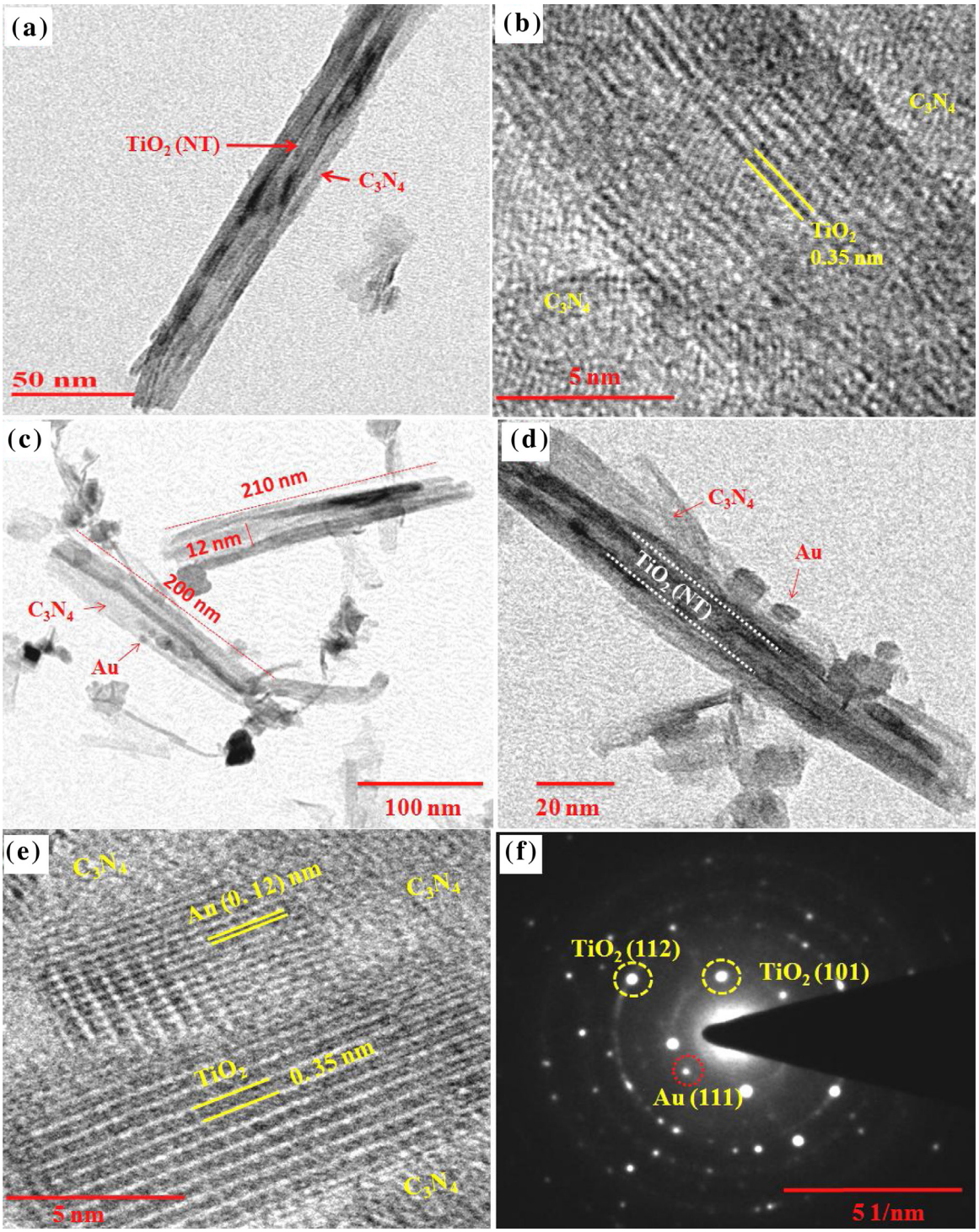

Fig. 2. HRTEM analysis of **(a, b)** C_3N_4-TiO_2 and **(c, d, e)** CTA-1 (Au, 0.75 wt%, C_3N_4:TiO_2 1:10) photocatalysts **(e)** SAED pattern of CTA-1 photocatalysts.

recorded on commercial Omicron EA 125, source Al-kα radiation at 1486.6 eV and the Raman spectra was analyzed by Airix (STR500). Surface area and porosity by BET, BEL mini-II, (Micro Trac Corp. Pvt. Ltd, Tokyo, Japan) based N_2 adsorption-desorption method at cryogenic temperature. The interfacial potential voltage (I–V) characteristics were recorded on KEITHLEY (4200-SCS) with ZYVEX S100 nanomanipulator.

The photocatalytic activity was carried out in a Pyrex tube (20 mL), containing the reaction mixture (water: MeOH, 4:1) and 0.03 g of photocatalyst under direct sunlight with intermittent stirring. Methanol was chosen to act as a sacrificial agent and hole scavenger. The mixture was purged before with argon gas for 20 min to create an inert atmosphere and irradiated under direct solar irradiation with an average solar flux of (330–750 Wm^{-1}) and average 25 °C temperature. The quantification of H_2 evolved during the reaction was done by gas chromatography (GC, Nucon Ltd, India) with thermal conductivity detector (TCD) and molecular sieve column (5X A, 1m). The temperature of oven, injector and detector was set at room and the injection was done manually by a gas tight syringe (Hamilton, 5 mL), the quantification of the evolved

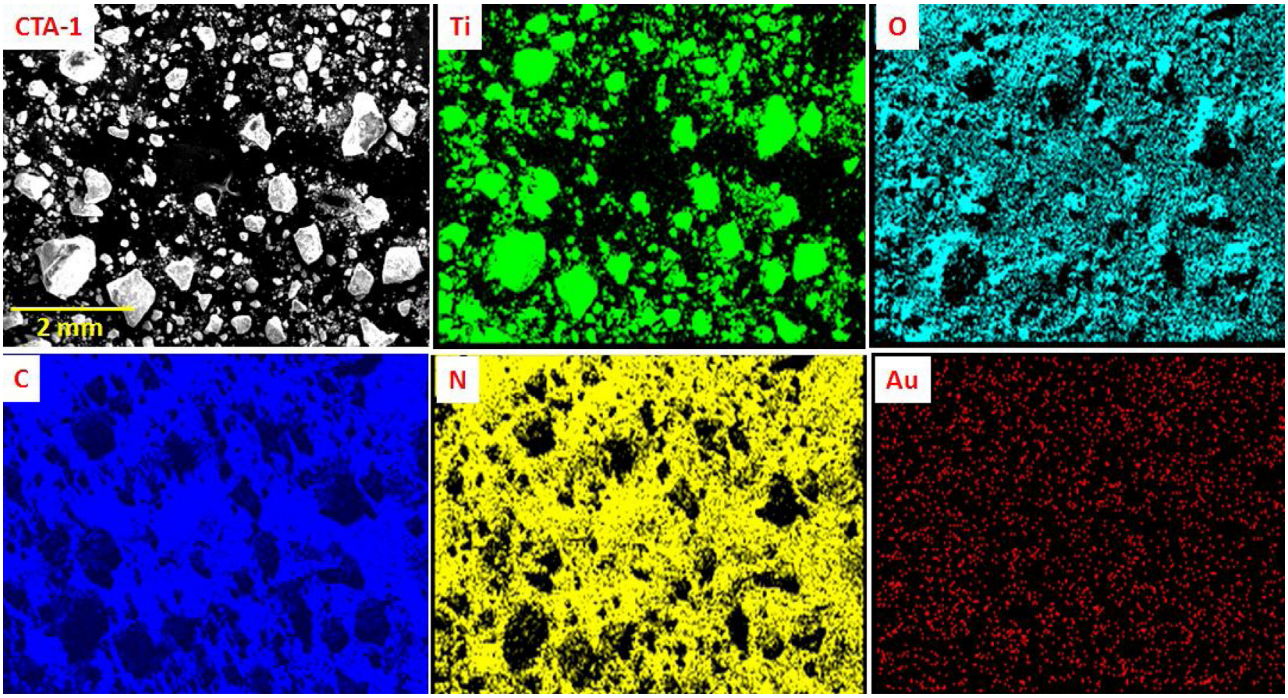

Fig. 3. EDS mapping of different elements present in CTA-1 (Au, 0.75 wt% and C_3N_4:TiO_2 1:10) photocatalyst.

gas was done in comparison to standard 180 PPM (N_2 balanced) H_2 gas standard (Sigma gases, India).

3. Results and discussion

3.1. Structural and morphological characteristics

The X-ray diffraction studies of the as prepared photocatalysts displayed the presence of anataseTiO_2 passivated with a layer of C_3N_4. As shown in Fig. 1 all the samples give the clear signals for the C_3N_4 and TiO_2 (anatase) without the presence of any trace impurity. The C_3N_4 displayed a characteristic peak around 27.3° attributed to 002 plane of carbon (JCPDS card No. 75-1621) which reflects the formation of layer of C_3N_4 over TiO_2 nanotubes due to interlayer stacking of aromatic rings [22], it can be concluded preliminarily that the bulk C_3N_4 has been exfoliated as a single thin layer coating over TiO_2 (NT) that was later confirmed by Raman spectroscopy. The diffraction pattern of the TiO_2 showed several peaks assigned to different planes of anatase polymorph, predominantly the formation of peak at 25.3° corresponding to (101) plane and several other peaks like 38.2° (112), 48° (200), 53.9° (105), 62.1° (612) and 70.3° (220) (JCPDS card No. 73-1764). The particle size of the tubular nanostructure was found to be larger in case of CTA-4, CTA-5 (Figure ESI-2) ascribed to the increase in C_3N_4 content resulting in the particle agglomeration. Moreover, the separate diffraction peak for the Au was not witnessed in the pattern though increase in the intensity of 38.2° peak can be attributed to the presence of Au (JCPDS card no.01-1172) and the low response to diffraction intensity can be due to its lower content of Au (<1 wt%) in all the samples [23,24].

The HRTEM results shown in Fig. 2 and Figure ESI-3 disclosed the 1D tubular type geometrical morphology of TiO_2 encapsulated by a monolayer of C_3N_4. The nanostructures are open ended having an average diameter of 12 nm and length 200–235 nm, the thickness of C_3N_4 layer is variable between 1 and 3 nm. Moreover, the Au nanoparticles are seen deposited on the surface of TiO_2 and also sandwiched in between C_3N_4 and TiO_2. The lattice fringes (d spacing) of CTA-1 photocatalyst have been measured to be 0.35 nm that

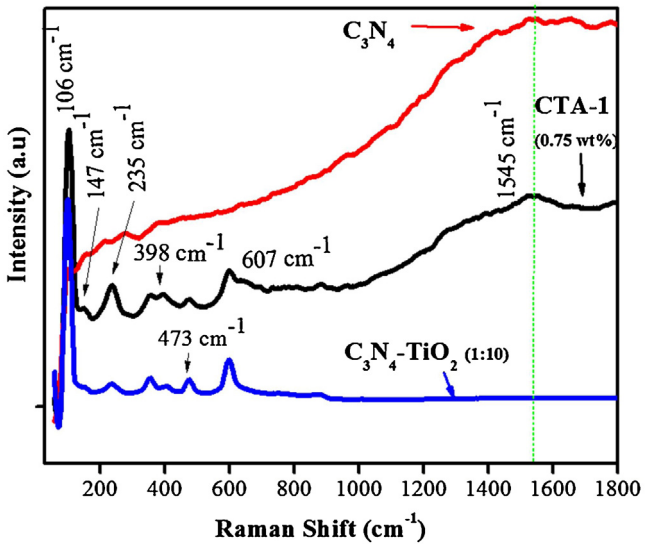

Fig. 4. Raman spectra of different photocatalysts.

is in consistence with the d spacing of (101) plane of TiO_2. The SAED pattern is also in consonance with the XRD and TEM results showing the tetragonal structure of TiO_2 unit cell and little amorphous nature after passivation with C_3N_4. The elemental ratio (Figure ESI-4) was found to be 0.74 wt%, which is in compliance to the expected ratio (0.75 wt%) and all the elements are spatially distributed as confirmed by elemental mapping (Fig. 3).

Raman scattering (Fig. 4) was specifically done to analyze the microstructures of the CTA-1 hybrid nanostructure showing the characteristics of anatase polymorph of TiO_2 and small shift in the intensity was observed after Au loading, peaks were observed around 106 cm^{-1}, 147 cm^{-1} (E_g), 398 cm^{-1}(B_{1g}), 473 cm^{-1} (B_{1g}) for both the C_3N_4-TiO_2 and CTA-1 related to the tetragonal structure of anatase TiO_2 with D_{4h} space group [25]. The band at 607 cm^{-1} is due to the Ti-O stretching vibration and the appearance of the G band

at 1545 cm^{-1} is due to the uniform coating of C_3N_4 on TiO_2, the formation of this band is ascribed to the formation of C_3N_4 layer and due to symmetric sp^2 stretching which imparts a graphitic nature to CTA-1. A significant increase in the intensity of a band around 235 cm^{-1} is due to interaction of Au with C_3N_4-TiO_2, earlier findings showed the similar change and related it to the basis for high electron transfer [26].

Figure ESI-5 represents the BET (Brunner-Emmet-Teller) based N_2 adsorption and desorption curves of the nanocatalysts, all the isotherms are typical type IV Langmuir due to the porous nature of the nanocomposites [27]. The C_3N_4 possessed a small surface area (81 m^2g^{-1}) and a huge pore diameter (80 nm) credited to the multilayer structure of C_3N_4 (FESEM, Figure ESI-3) and the pore distribution was non-uniform. As shown in the BJH curve (Barret-Joyner-Halenda) this non distribution turns out into uniform after tubular composite formation with TiO_2 attributed to the self exfoliation process of C_3N_4. As shown in Table ESI-1 the C_3N_4-TiO_2 possess highest surface area (139 m^2g^{-1}) that decreased after Au addition and was found to be 129 m^2g^{-1} due to the accumulation of Au particles into the pores of TiO_2 (NT) which also resulted in a little change in the pore volume (0.34 cm^3g^{-1} and 0.31 cm^3g^{-1} for CTA-1 and C_3N_4-TiO_2 respectively), in compliance to this the pore diameter decreased from 2.71 nm to 1.85 nm after Au loading. Furthermore, the specific surface area effectively decreased with the increase of C_3N_4 content due to aggregation of nanoparticles, the surface area of CTA-4 and CTA-5 was found to be 86.4 and 80.6 m^2g^{-1} respectively.

3.2. Optical and thermal characteristics

The optical properties of the photocatalysts were studied by UV–vis absorption spectroscopy (Fig. 5). It is evident that the as synthesized C_3N_4 showed strong response to visible light (440 nm) due to its lower band gap (2.6 eV), after its encapsulation on TiO_2 and simultaneous Au loading the NC showed a blue shift, the absorption edge of C_3N_4-TiO_2 and CTA-1 was observed at 417 and 411 nm respectively. The expected blue shift is credited to the charge transfer from the C_3N_4 towards the E_{CB} of TiO_2 and quantum confinement effect. Moreover, the bare Au nanoparticles (Au NP's) showed a strong absorption maximum at 525 nm (Figure ESI-6) due to the surface plasmon resonance (SPR) effect [28], the band shifted to little higher λ_{max} (550 nm) after the incorporation of Au on C_3N_4-TiO_2. The band gap (E_g) calculated as per Tauc equation was found to be 2.6, 2.9 and 3.0 eV respectively for C_3N_4, C_3N_4-TiO_2 and CTA-1 photocatalyst. There was little change in absorption maximum of the NC by changing the C_3N_4 ratio (CTA-4, and CTA-5) while as the intensity of SPR band was found to be dependent on the weight ratio of Au (Figure ESI-7), a low intensity SPR absorption band was observed in case of 0.25 wt% Au (CTA-3) that increased respectively for 0.50 wt% (CTA-2) and 0.75 wt% (CTA-1).

The thermal gravimetric analysis (TGA) analysis revealed a good thermal stability of the photocatalysts (Figure ESI-8). It was observed that in comparison to bare C_3N_4 there was a negligible weight loss in C_3N_4-TiO_2 and CTA-1 nanocatalysts up to 500 °C under N_2 atmosphere. Two breaks were observed in the TGA curve at 70 °C and 137 °C due to moisture loss and exclusion of adsorbed gases respectively. This result is in consonance with the earlier results showing the thermal stability of C_3N_4-TiO_2 NC up to 500 °C [14].

3.3. X ray photon spectroscopy (XPS) and potential voltage (I–V) characteristics

The chemical state and surface composition was recorded by XPS and the survey spectrum is presented in Fig. 6. The survey spectrum of CTA-1 (Fig. 6a) showed that the hybrid tubular nanocomposite is composed of elements like C, N, Ti, O and Au. In C1s spectrum two separate peaks were observed at 284.8 eV and 287 eV. The main peak around 287 eV is assigned to C—N—C and the C—$(N)_3$ group of C_3N_4 and the other deconvulated peak at 284.8 eV is assigned to C—C sp^2 hybridization [30]. The high resolution N1s spectra is also fitted into two peaks of the binding energy 399.7 eV and 396.2 eV credited to $C(N)_3$ and C—N—C respectively. The O1 s spectrum is fitted in two deconvulated peaks with binding energy values at 530.6 eV and 531.5 eV which are directly ascribed to the TiO_2 and H_2O respectively, supported by earlier finding [29]. In case of Ti2p two binding energy values are recorded at 459.2 eV and 464.2 eV assigned to two typical state of Ti^{+4} ($2p_{3/2}$ and $2p_{1/2}$ respectively). Moreover, an interesting satellite peak was observed at a binding energy value (457.2 eV) of Ti^{+3} $2p_{3/2}$ and at 463.5 eV for Ti^{+3} $2p_{1/2}$ respectively and these peaks are ascribed to the possible formation of some Ti^{+3} ($2p_{3/2}$) species. This finding is in compliance to earlier finding [20,30], Liyan Shen et al. reported [30] that the presence of reducing agent in the same mixture reduces some of the Ti^{+4} species to Ti^{+3} and in the current synthesis the mixture contains ascorbic acid that might have helped in the formation of some Ti^{+3} species giving rise to a shoulder peaks (457.5 eV and 463.5 eV). The XPS spectrum of Au is fitted into two major peaks at 84.1 eV and 87.6 eV assigned to typical $4f_{5/2}$ and $4f_{7/2}$ of elemental Au and a small peak at 85.5 eV is assigned to Au (III) oxidation state.

The electric properties of the C_3N_4, C_3N_4-TiO_2 and CTA-1 are presented in Fig. 7 signifying the typical semiconductor nature of the nanocatalysts. With the applied voltage the CTA-1 heterojunction showed the higher conductivity (1.385×10^{-4} A) in comparison to C_3N_4-TiO_2 (8.04×10^{-5} A) and C_3N_4 (2.65×10^{-9} A). It has been observed that the apparent curve of C_3N_4 (Fig. 7 inset) is showing an ohmic behavior while as after composite formation the non-ohmic properties developed and the junction showed higher current efficiency due to the effective transfer and enhanced life time of electrons along the inbuilt junction [31]. An asymmetrical rectifying response has been observed indicating the existence of Schottky barrier in the heterojunction. In case of CTA-1 the ternary junction develops little ohmic properties compared to C_3N_4-TiO_2 due to effective quenching of electrons towards Au surface.

3.4. Photocatalytic activity

Before studying the photocatalytic hydrogen evolution under sunlight several control experiments were performed for the optimization of reaction condition. Photolysis (without the catalyst) and dark experiments showed no traces of H_2 evolution indicating that H_2 evolution is merely due to the photocatalysis process. The content of Au loading (wt%) was optimized by the photoluminescence (PL) studies (Figure ESI-9a). It has been observed that 0.75 wt% of Au loaded on C_3N_4-TiO_2 showed the maximum quenching followed by 0.50 wt% and 0.25 wt%. The quenching is attributed to the effective separation of charge carriers, caused due to shuttling of electrons towards metal atoms [32]. So, 0.75 wt% of Au was considered as an optimized amount for the effective H_2 evolution. Furthermore, in compliance to our earlier report [33] here it was also observed that 0.006 g/mL of the catalyst dispersed in the reaction mixture showed the highest H_2 evolution (Figure ESI-9b).

As presented in Figure ESI-10 several hole scavenging/sacrificial donors were used to check the better compatibly regarding the performance of the nanocatalysts for the half reduction of H_2O. Methanol (CH_3OH) has been found to be efficient for the H_2 evolution in comparison to Na_2CO_3, Na_2SO_4, and EDTA. Moreover, it is also found that after 5 h of sunlight irradiation using CH_3OH (5 mL) produced 250 μmols of H_2 while as a mixture (H_2O:CH_3OH 4:1) the H_2 evolution rate increases, mainly due to the reason that CH_3OH not only acts as a hole scavenger but also as a sacrificial

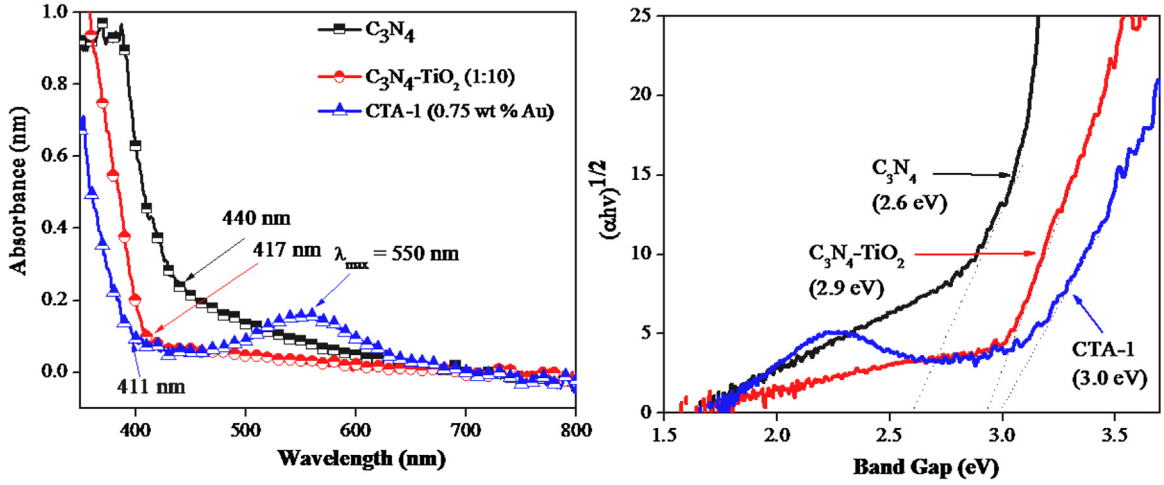

Fig. 5. Optical absorption spectra and band gap (Eg) calculated by Tauc equation of different photocatalyst.

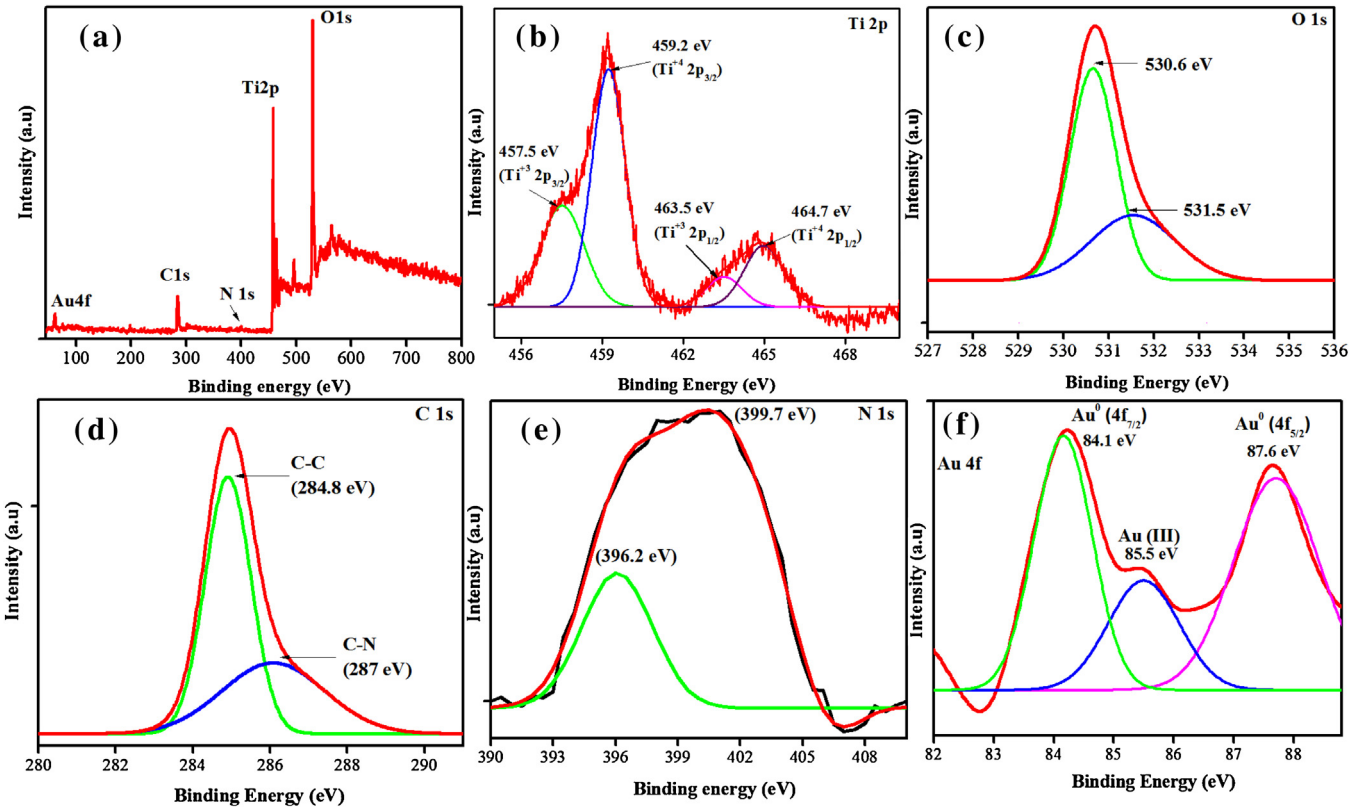

Fig. 6. XPS analysis of the tubular C_3N_4-Au-TiO_2 photocatalyst **(a)** Survey Spectrum **(b)** Ti 2p **(c)** O 1s **(d)** C 1s **(e)** N 1s **(f)** Au 4f.

donor resulting in the formation of intermediates like formic acid (HCOOH) or formaldehyde (HCHO) [34] who are indirectly involved in the photocatalytic reduction of H^+ produced during water splitting reaction.

The H_2 evolution reaction rates with different photocatalyts are shown in Fig. 8a, the bare C_3N_4 do not show any response to H_2 evolution due to its ineffectiveness for the separation of charge carriers (e^-/h^+) [35]. Compared to TiO_2 the C_3N_4 possess more negative reduction potential (*vs* normal hydrogen electrode, NHE) [29] due to which the transfer of electrons take place from of C_3N_4 (E_{CB}) to TiO_2 (E_{CB}) and the nanocomposite (C_3N_4-TiO_2) becomes active for the H_2 evolution resulting in the evolution of 35 μmol of gas under direct sunlight (5 h). In case of the bare Au NP's little H_2 (39 μmol) evolution was also observed. After the incorporation of Au, the rate of H_2 production increased and it was observed that the CTA-1 photocatalyst produced almost 450 μmols of H_2, showing a decrease in case of CTA-2 (170 μmols) and CTA-3 (45 μmols) due to lower Au content, in accordance to the PL results the higher activity of CTA-1 is directly related to the effective separation of charge carriers due to shuttling of the electrons in three component system (CTA), also complies with the earlier results [36] and further correlated to the surface plasmon resonance (SPR) effect of Au leading to the activation of Au atoms, so Au acts both as a sensitizing agent for to TiO_2 and also acts as a co-catalyst and helps in the transport of electrons. The H_2 evolution was witnessed to decrease by keeping the Au content constant (0.75 wt%) and varying the ratio of C_3N_4. It is observed

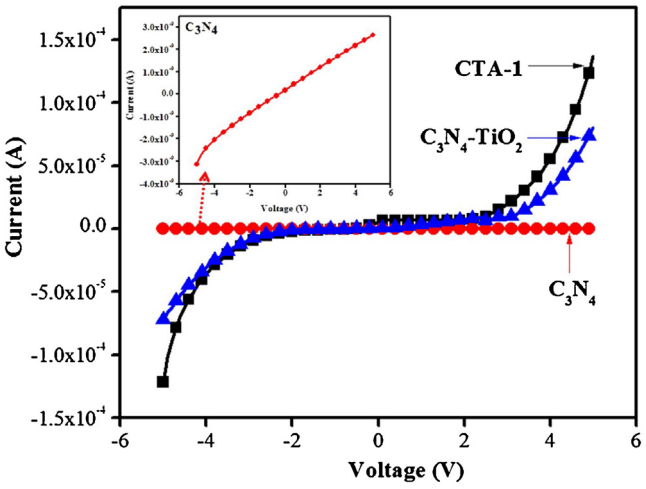

Fig. 7. Potential voltage (I-V) characteristics of the nanostructures.

that CTA-4 and CTA-5 produced 210 μmols and 175 μmols of H_2 respectively. The decrease in the activity with the increase of C_3N_4 content is expected due to agglomeration of the nanoparticles resulting in the decrease of their specific surface area (Table ESI-1). The time course study of CTA-1 (Fig. 8b) upto 9 h showed an exponential increase in the H_2 production (88 μmolh^{-1}). Furthermore, the role of sunlight flux (Wm^{-1}) was also studied (Figure ESI-11) and it was found that the solar irradiance has least effect on H_2 production upto 400 Wm^{-1}. It has been reported earlier [33] that the rate of reaction slowed down when the sun irradiance flux goes below 300 Wm^{-1}. The higher photocatalytic activity of CTA over C_3N_4-TiO_2 and bare C_3N_4 is mainly due to two reasons; one is the synergistic effect of Au and second is the perfect band alignment after the formation of ternary heterojunction. Under direct solar light irradiation which constitutes 45% of the visible light portion, Au is activated due to its SPR effect and simultaneously C_3N_4 is also activated because of its lower E_g (2.6 eV). The reduction of H^+ is expected to take place on the TiO_2 (NT) surface due to its matching E_{CB} potential (-0.29 Vs NHE) to the half reduction of water splitting reaction [13]. Furthermore, in order to explore the intrinsic role of different components the photocatalytic reaction was carried under several monochromatic wavelengths like 514 nm, 457 nm, 488 nm and 314 nm (reaction setup is shown in Figure ESI-12) and as shown in Figure ESI-13 it was observed that the 457 nm wavelength produces highest amount of H_2 (112 μmol) followed by 488 nm (62 μmol) and 514 nm (32.25 μmol) and little response was also observed under 314 nm (31 μmol) wavelength. These results disclose the activation of C_3N_4 occurs under visible light due to its lower band energy and is more dominating in order to sensitize the TiO_2 compared to Au, similarly it was observed that the TiO_2 itself is also activated under UV light with a low response to the H_2 production.

As shown in Scheme 1 when the NC is irradiated under sunlight irradiation, the electrons from E_{VB} (valance band) of C_3N_4 and TiO_2 are excited to their respective E_{CB} and simultaneously due to SPR effect Au nanoparticles are also activated. The I–V characteristics suggested the non ohmic properties of the heterojunction and in accordance with the HRTEM analysis it is presumed that the comparative work function of C_3N_4 (4.31), Au (5.1) and TiO_2 (4.9) causes the Fermi level equilibration between Au-TiO_2. So, at C_3N_4-TiO_2 interface the electrons move easily towards the E_{CB} of TiO_2 via Au, this mechanism is also supported by earlier studies reported by Yanfeng Chen et al. [13]. Secondly, the band potential of C_3N_4 (−1.12 eV Vs NHE for E_{CB}) is more negative than TiO_2 (E_{CB} = −0.29 Vs NHE), the photo induced electrons easily pass the interface and are transferred to the E_{CB} of TiO_2, simultaneously the holes produced in the TiO_2 under UV excitation are transferred to E_{VB} of C_3N_4 promoting the charge carrier separation and enhance the photocatalytic activity for H_2 production. Moreover, the presence of Ti^{+3} in the CTA-1 nanostructure due to expected reduction of fewer Ti^{+4} are able to enhance the rate of the photocatalytic reaction [20,30].

Methanol scavenges the holes and gets oxidized to formic acid or formaldehyde, which by indirect means boosts the half reduction of H_2O molecule to produce H_2. Furthermore, the rate of H_2 produced *vs* surface area has been normalized and presented in Fig ESI-13, it was observed that the CTA-1 nanocomposite produced 24.2 μmol$h^{-1}m^{-2}$ of H_2 followed by CTA-4 (17.42 μmol$h^{-1}m^{-2}$) and CTA-5 (13.51 μmol$h^{-1}m^{-2}$). The higher photocatalytic hydrogen production by CTA-1 photocatalyst is credited to better charge delocalization due to its high specific surface area and its mesoporous nature that enhances the binding ability of the reactants and also helps in efficient ionic transport along the elongated 1D surface with high aspect ratio.

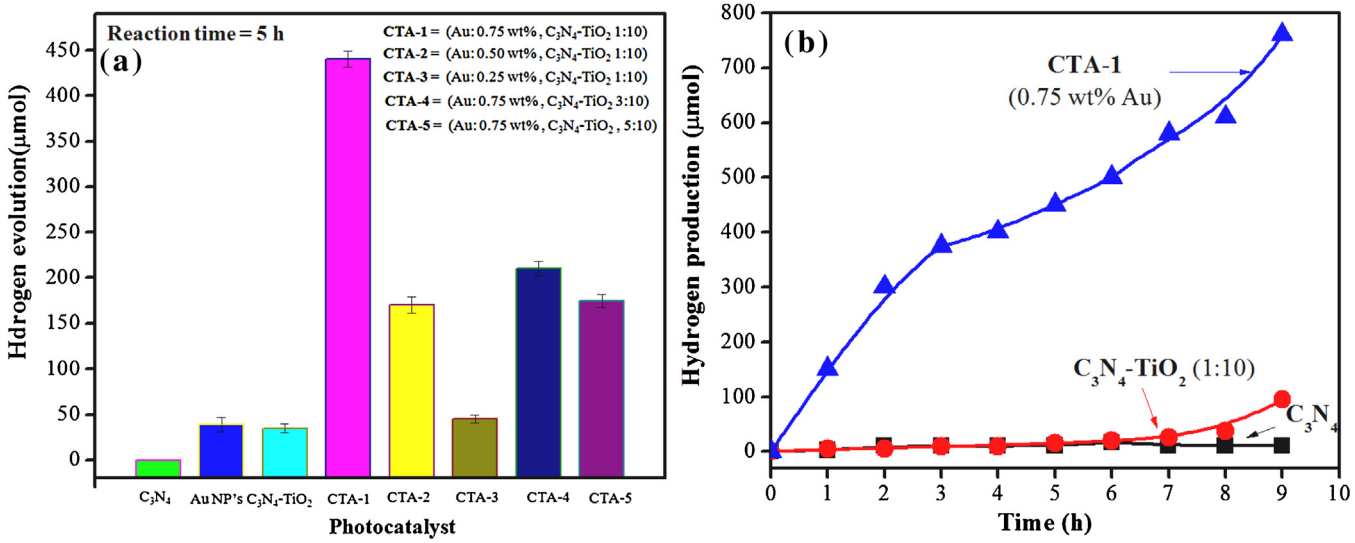

Fig. 8. (a) Photocatalytic H_2 production from water by different photocatalysts under sunlight irradiation (b) Time course photocatalytic hydrogen production by different photocatalysts.

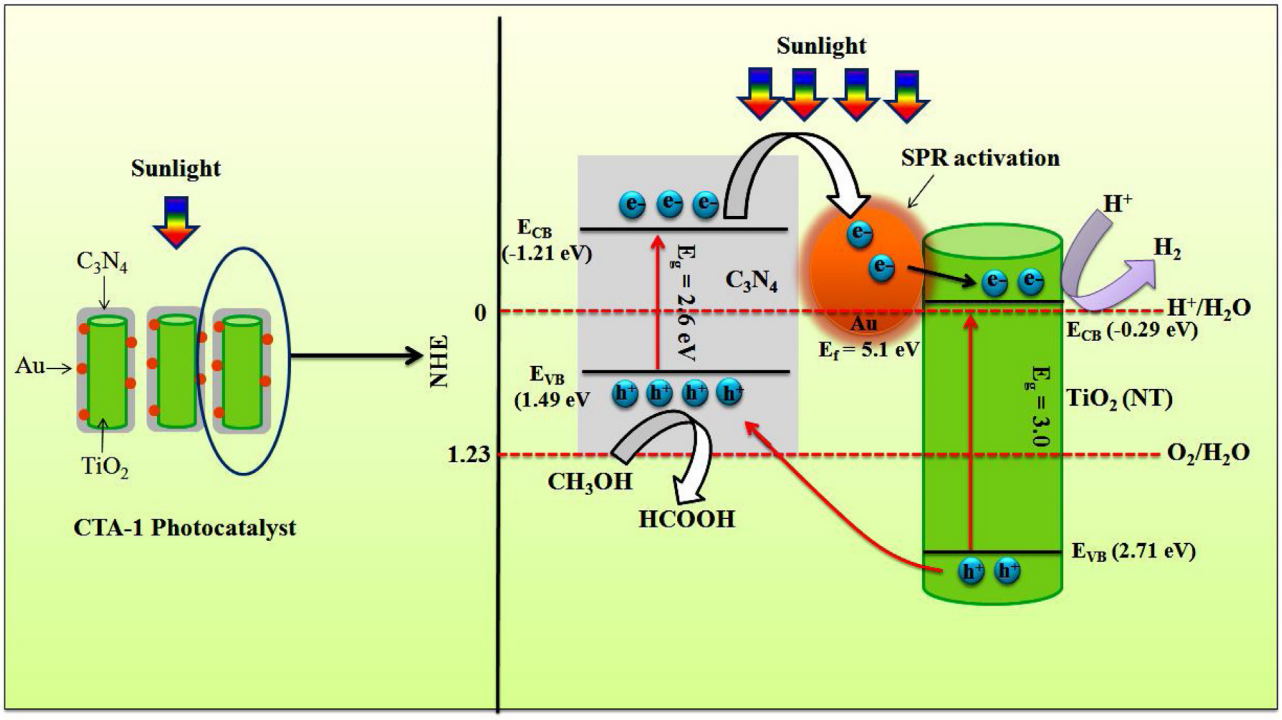

Scheme 1. Proposed mechanism for the H_2 production from water by C_3N_4-Au-TiO_2 (CTA-1) photocatalyst.

The stability of the CTA-1 photocatalyst has been observed by doing the recycling for 3 consecutive cycles with a minimum loss (<1%) in over all activity (Figure ESI-14). The optical absorption analysis (Figure ESI-15) of the recycled photocatalyst didn't show any major destabilization confirming the photostability and long term applicability of the material.

4. Conclusion

In summary the assembled C_3N_4 passivated Au-TiO_2 tubular nanostructure was found active in direct solar light for the efficient H_2 production from half water splitting reaction. The embedment of TiO_2 (NT) by a thin monolayer C_3N_4 causes the heterogeneous nucleation and the simultaneous Au loading resulted in the formation of an efficient sunlight activated NC. The Au sensitizes the NC and also shows co catalytic activity. Sunlight activates both the C_3N_4 and Au and the formation of non ohmic heterojunction helps in the electron transfer along C_3N_4/Au-TiO_2 interface, simultaneously due to more negative reduction potential of C_3N_4 (E_{CB}) electrons are transferred to E_{CB} of TiO_2 (NT) resulting in the efficient charge separation with a remarkable photocatalytic H_2 evolution. The futuristic agenda of the work is the in process utilization of the H_2 produced for the reduction of industrially important nitro aromatics and hydrogenation reactions.

Acknowledgements

The authors are highly thankful to the material research center (MRC) MNIT Jaipur, Sai labs Thapar University Patiala, for the characterization of the NC. Thanks are due to Dr S. K. Mittal (Pollution monitoring lab, Thapar University) and Dr. Soumen Basu of our School for providing the sunlight irradiance data and BET analysis respectively.

Appendix A. Supplementary data

Supplementary data associated with this article can be found, in the online version, at http://dx.doi.org/10.1016/j.apcatb.2017.05.002.

References

[1] K. Shimura, H. Yoshida, Energy Environ. Sci. 4 (2011) 2467–2481.
[2] A. Kudo, Y. Miseki, Chem. Soc. Rev. 38 (2009) 253–278.
[3] H. Park, H.-i. Kim, G.-h. Moon, W. Choi, Energy Environ. Sci. 9 (2016) 411–433.
[4] X. Chen, S. Shen, L. Guo, S.S. Mao, Chem. Rev. 110 (2010) 6503–6570.
[5] M. Ni, M.K. Leung, D.Y. Leung, K. Sumathy, Renew. Sustain. Energy Rev. 11 (2007) 401–425.
[6] J. Tian, Z. Zhao, A. Kumar, R.I. Boughton, H. Liu, Chem. Soc. Rev. 43 (2014) 6920–6937.
[7] S. Hernández, D. Hidalgo, A. Sacco, A. Chiodoni, A. Lamberti, V. Cauda, E. Tresso, G. Saracco, Phys. Chem. Chem. Phys. 17 (2015) 7775–7786.
[8] A.L. Linsebigler, G. Lu, J.T. Yates Jr., Chem. Rev. 95 (1995) 735–758.
[9] H. Li, Z. Bian, J. Zhu, Y. Huo, H. Li, Y. Lu, J. Am. Chem. Soc. 129 (2007) 4538–4539.
[10] A. Wolcott, W.A. Smith, T.R. Kuykendall, Y. Zhao, J.Z. Zhang, Small 5 (2009) 104–111.
[11] J.M. Macak, M. Zlamal, J. Krysa, P. Schmuki, Small 3 (2007) 300–304.
[12] H. Yan, H. Yang, J. Alloys Compd. 509 (2011) L26–L29.
[13] Y. Chen, W. Huang, D. He, Y. Situ, H. Huang, ACS Appl. Mater. Interfaces 6 (2014) 14405–14414.
[14] J. Yan, H. Wu, H. Chen, Y. Zhang, F. Zhang, S.F. Liu, Appl. Catal. B: Environ. 191 (2016) 130–137.
[15] S. Sarina, E.R. Waclawik, H. Zhu, Green Chem. 15 (2013) 1814–1833.
[16] Z.W. Seh, S. Liu, M. Low, S.Y. Zhang, Z. Liu, A. Mlayah, M.Y. Han, Adv. Mater. 24 (2012) 2310–2314.
[17] J. Li, S.K. Cushing, P. Zheng, T. Senty, F. Meng, A.D. Bristow, A. Manivannan, N. Wu, J. Am. Chem. Soc. 136 (2014) 8438–8449.
[18] M. Yang, J. Liu, X. Zhang, S. Qiao, H. Huang, Y. Liu, Z. Kang, Phys. Chem. Chem. Phys. 17 (2015) 17887–17893.
[19] C. Miranda, H. Mansilla, J. Yáñez, S. Obregón, G. Colón, J. Photochem. Photobiol. A: Chem. 253 (2013) 16–21.
[20] K. Li, S. Gao, Q. Wang, H. Xu, Z. Wang, B. Huang, Y. Dai, J. Lu, ACS Appl. Mater. Interfaces 7 (2015) 9023–9030.
[21] A. Nakahira, T. Kubo, C. Numako, Inorg. Chem. 49 (2010) 5845–5852.
[22] J. Zhang, M. Grzelczak, Y. Hou, K. Maeda, K. Domen, X. Fu, M. Antonietti, X. Wang, Chem. Sci. 3 (2012) 443–446.
[23] S. Zhu, S. Liang, Q. Gu, L. Xie, J. Wang, Z. Ding, P. Liu, Appl. Catal. B: Environ. 119 (2012) 146–155.

[24] R.A. Rather, S. Singh, B. Pal, J. Ind. Eng. Chem. 37 (2016) 288–294.
[25] X. Zhang, F. Wang, H. Huang, H. Li, X. Han, Y. Liu, Z. Kang, Nanoscale 5 (2013) 2274–2278.
[26] K. Yang, C. Meng, L. Lin, X. Peng, X. Chen, X. Wang, W. Dai, X. Fu, Catal. Sci. Technol. 6 (2016) 829–839.
[27] D. Chen, F. Huang, Y.B. Cheng, R.A. Caruso, Adv. Mater. 21 (2009) 2206–2210.
[28] G. Baffou, R. Quidant, Chem. Soc. Rev. 43 (2014) 3898–3907.
[29] B. Chai, T. Peng, J. Mao, K. Li, L. Zan, Phys. Chem. Chem. Phys. 14 (2012) 16745–16752.
[30] L. Shen, Z. Xing, J. Zou, Z. Li, X. Wu, Y. Zhang, Q. Zhu, S. Yang, W. Zhou, Sci. Rep. 7 (2017).
[31] L. Guo, Y. Hu, B. Yu, E. Davis, R. Irvin, X. Yan, D. Li, Scientific Reports 6, 2016.
[32] R.A. Rather, S. Singh, B. Pal, Sol. Energy Mater. Sol. Cells 160 (2017) 463–469.
[33] R.A. Rather, S. Singh, B. Pal, J. Catal. 346 (2017) 1–9.
[34] H.-J. Choi, M. Kang, Int. J. Hydrogen Energy 32 (2007) 3841–3848.
[35] P. Wu, J. Wang, J. Zhao, L. Guo, F.E. Osterloh, J. Mater. Chem. A 2 (2014) 20338–20344.
[36] H. Tada, T. Mitsui, T. Kiyonaga, T. Akita, K. Tanaka, Nat. Mater. 5 (2006) 782–786.